Nuclear Instruments and Methods in Physics Research B44 (1989) 184–194
North-Holland

DETERMINATION OF CONCENTRATION PROFILES BY ELASTIC RECOIL DETECTION WITH A ΔE–E GAS TELESCOPE AND HIGH ENERGY INCIDENT HEAVY IONS

J.P. STOQUERT, G. GUILLAUME, M. HAGE-ALI, J.J. GROB, C. GANTER and P. SIFFERT

Centre de Recherches Nucleaires and Université Louis Pasteur, F-67037 Strasbourg Cedex, France

Received 7 January 1989 and in revised form 23 June 1989

The Elastic Recoil Detection (ERD) method has been used to determine the profile of a wide range of elements simultaneously in a thin layer (1 μm) with a depth resolution of a few hundred Å and high sensitivity. Z separation is achieved by a ΔE(gas)–E(solid) telescope. Results for ^{127}I (up to 240 MeV) incident ions used to profile thin films of dielectrics ($SiO_xN_yH_z$), amorphous semiconductors (a-GaAs : H) and superconductors (YBaCuO, BiSrCaCuO) are reported. It has been considered previously that ERD is of interest for analysis of light elements. We show that high energy heavy incident ions extend the field of application of the ERD method to all elements with an approximately constant depth resolution and sensitivity.

1. Introduction

MeV ion-beam analysis with light ions has been demonstrated to be a powerful technique for sensitive measurements of atomic profiles in the near surface region (1 μm) of solids. Particularly, Rutherford backscattering (RBS) with low energy ^{4}He ions has been extensively used. A major difficulty however arises in this method, essentially for light elements, due to peak overlapping in many cases of practical interest. One possibility to overcome this difficulty consists of measuring the depth profile using a specific nuclear reaction (NR) for a given element.

L'Ecuyer et al. [1] proposed the elastic recoil detection (ERD) technique to determine the concentration of light elements in heavy substrates, by using ^{35}Cl ions of 30 MeV and absorbers before the detector in order to discriminate between scattered ions and recoiling atoms. Separate determinations of concentration for atoms with different masses have been obtained with heavy incident ions and simultaneous measurements of the scattered and recoiling atoms, by Cohen et al. [2] for hydrogen, and with 30 MeV incident alpha particles by Klein [3] for some light elements, but the most commonly used ERD applications refer to low energy (2–3 MeV) ^{4}He incident ions for measurements of hydrogen concentration in various samples [4].

Recently, improvements in the ERD method have been introduced which make it possible to determine simultaneously the profile of several elements in a given thin film. Time-of-flight techniques [5] as well as gas telescope [6], magnetic spectrometer [7], quadrupole mass spectrometer [8] or a combination of time-of-flight and energy in a recoil telescope [9] have been used for this purpose.

Although particle identification spectrometers have been widely used in nuclear physics, they have been little used for analysis, and further investigations are necessary to demonstrate all the possibilities of these techniques. Until now, ERD measurements have been performed with light and intermediate ions at low and medium (about 50 MeV) energies [10,11], and only little data exist with recoil discrimination, restricting the applications to analysis of light elements [12], typically for $A < 30$.

We have investigated the possibilities of the ERD method with ^{58}Ni and ^{127}I at the 16 MV tandem accelerator of the Centre de Recherches Nucléaires at Strasbourg (CRN). We report here the results of high energy ^{127}I ions with 130 to 240 MeV incident energy which extend the technique to analysis of elements with higher Z values. For the Z-determination, we have used a gas telescope which offers advantages of compactness and simplicity in surface studies, as compared to other method of recoil discrimination. In particular, with gas telescopes, the geometry of detection can be easily adapted to specific cases.

Z discrimination by means of a gas telescope, for heavy ions ($A > 50$) needs high energies which cannot be transferred to the recoils by light incident ions in the pure Coulomb regime where the Rutherford scattering law applies. We therefore studied in detail the combination of a gas telescope with high energy heavy incident ions. Increase in the cross sections and in the energy losses with charge Z are expected to influence sensitivity and depth resolution in a favourable way, as well as

0168-583X/89/$03.50

the analysed depth which is also improved with higher energy. However, these variations are not independent, and a detailed discussion has to be undertaken.

2. Basic considerations and optimization of experimental conditions

Although theoretical expressions which relate energy to depth and concentration for ERD are known and quite similar to those for RBS, different formulae have been derived for the resolution, depending on the sources of dispersion which have been considered. In the following, we describe the formalism which has been used for one monolayer in order to make comparisons possible with other experimental conditions. For this purpose, we define a standard set of experimental parameters (scattering geometry, solid angles, beam dose) from which a theoretical estimate of the sensitivity and resolution is possible for different incident ions and energies.

2.1. Geometry

The experimental configuration is shown schematically in fig. 1. In the laboratory frame, a monoenergetic ion beam of energy E_0 collimated to a diameter of 2 mm is incident on a solid target at an angle α with respect to the surface. Target atoms recoil at an angle $\alpha + \beta$ where β is the glancing angle between the surface and the detector direction, with energy E_k given by

$$E_k = kE_0, \tag{1}$$

where k is the kinematic factor:

$$k = \frac{4M_1M_2}{(M_1+M_2)^2}\cos^2(\alpha+\beta). \tag{2}$$

M_1 and M_2 being the masses of the incident ion and target atom respectively ($k = 0$ for $\alpha + \beta > 90°$).

For $M_1 > M_2$, the elastically scattered projectiles are within a cone of half-angle θ_{max}:

$$\theta_{max} = \arcsin\frac{M_2}{M_1}. \tag{3}$$

In order to prevent excessive dead time and energy overlap due to the large elastic yield coming from the scattered beam, the recoil angle is chosen greater than θ_{max} [13]. The effective detection geometry results from a compromise between constraints related to cross-sections, stopping powers and energy spread which vary with the angles as shown below.

2.2. Depth scale

The analysed depth depends on the incident energy. Consider the case where the atoms recoil from a depth x beneath the surface; their energy $E_s(x)$ before reaching the telescope, is

$$E_S(x) = kE_0 - \{S\}x. \tag{4}$$

The recoiling factor $\{S\}$ is defined by

$$\{S\} = \frac{kS_1}{|\sin\alpha|} + \frac{S_2}{|\sin\beta|}, \tag{5}$$

where S_1 and S_2 are the mean stopping powers

$$\frac{1}{x}\int_x^0 \frac{dE}{dx}dx$$

for the incoming and outcoming ions, respectively.

The residual energy of the atom reaching the solid detector $E_R(s)$ is:

$$E_R(x) = E_s(x) - \Delta E_T(x), \tag{6}$$

where $\Delta E_T(x)$, the energy loss in the ionization chamber, described in section 3.2, is the sum of two terms corresponding to the entrance foil and to the gas, both

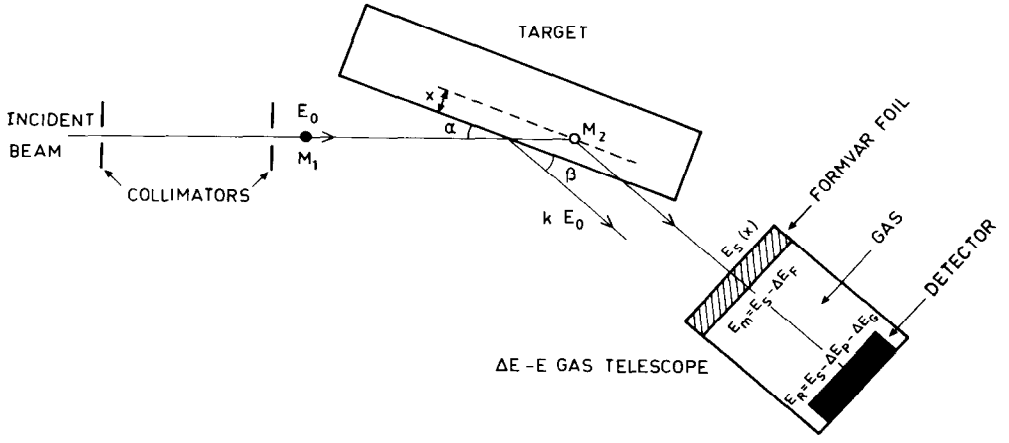

Fig. 1. Schematic view of the experimental setup.

depending on the energy and on the charge of the atom.

$$\Delta E_T(x) = \Delta E_F(x) + \Delta E_G(x). \quad (7)$$

E_R and ΔE_G are measured simultaneously, ΔE_F and $\{S\}$ can be calculated from tables from Ziegler [24], by using Bragg's additivity rule if necessary. Finally, the total measured energy

$$E_m = E_R + \Delta E_G \quad (8)$$

is related to depth x, and the energy to depth conversion factor η is defined for each type of recoiling atoms as

$$\eta = \frac{dE_m}{dx} = \frac{d(E_R + \Delta E_G)}{dx} = \frac{d(E_s - \Delta E_F)}{dx}. \quad (9)$$

2.3. Depth resolution

For a monoenergetic incident beam, the nuclei recoiling from depth x are registered with an energy width W in the detecting system. The depth resolution r is defined as

$$r(x) = W(x)/\eta(x). \quad (10)$$

The energy spreads which contribute to the total resolution are

i) the energy width δE_0 of the incident beam;
ii) the intrinsic detector resolution δE_D which is the quadratic sum of the electronic noise and of the E and dE detectors resolution;
iii) the geometrical broadening due to finite detector acceptance angle which causes kinematic factor variation and path length differences. Angular variations $\delta\alpha_0$ and $\delta\beta_0$ contribute to δE_m for $\delta E_{\alpha 0}$ and $\delta E_{\beta 0}$, respectively;
iv) the energy straggling δE_B in the target and the inhomogeneities and straggling in the telescope entrance foil;
v) the multiple scattering in the target and in the telescope entrance foil, which causes angular and lateral spread and adds to the geometrical broadening.

The total energy resolution is then expressed as:

$$\delta E_m^2 = (k\delta E_0)^2 + \delta E_D^2 + \delta E_\alpha^2 + \delta E_\beta^2 + \delta E_B^2. \quad (11)$$

From eqs. (4)–(8) one deduces the geometrical broadening

$$\delta E_\alpha = \left[-2kE_0 \tan(\alpha+\beta) + \frac{2xS_1}{\sin\alpha} \tan(\alpha+\beta) + kx\frac{S_1}{\sin\alpha}\cot\alpha \right] \delta\alpha, \quad (12)$$

$$\delta E_\beta = \left[-2kE_0 \tan(\alpha+\beta) + \frac{2kxS_1}{\sin\alpha} \tan(\alpha+\beta) + x\frac{S_2}{\sin\beta}\cot\beta \right] \delta\beta \quad (13)$$

and the total straggling is

$$\delta E_R^2 = 8 \ln 2 \left[\frac{k\Omega_i^2}{\sin^2\alpha} + \frac{\Omega_0^2}{\sin^2\beta} + \Omega_F^2 \right], \quad (14)$$

where Ω_i, Ω_0 and Ω_F are the energy straggling in the target during the incoming and outgoing path and in the telescope entrance foil, respectively. It can be noticed that the choice of E_m limits the straggling effects (E_R contains also the straggling in gas).
Ω can be estimated from Bohr's calculation

$$\Omega^2 = 4\pi Z_1^2 Z_2 e^4 N t \quad (15)$$

for a particle of charge $Z_i e$ traversing a medium of thickness t with NZ_2 electrons per unit of volume.

The angular fluctuations depend on the geometry of the detecting system and on multiple scattering in the target and in the telescope entrance foil. If the incident beam is collimated to be parallel ($\delta\alpha_0 = 0$), the geometrical contribution at the surface is limited to

$$\delta\beta_0^2 = \frac{1}{16D^2}\left(s^2 + d^2 \frac{\sin^2\beta}{\sin^2\alpha} \right), \quad (16)$$

where D is the distance between detector and target, s is the width of the detector circular aperture and d is the incident beam width defined by the diameter of the collimator.

Angular dispersion and lateral spread due to multiple scattering depend on the depth and can be calculated from the Tables of Sigmund and Winterbon [14] and Marwick and Sigmund [15] and quadratically added to the surface term at each depth:

$$\delta\beta^2 = \delta\beta_0^2 + \delta\beta_{m.s.}^2 \quad \delta\alpha = \delta\alpha_{m.s.} \quad (17)$$

Calculations for incident ions of ^{127}I in different cases are represented in fig. 2 and compared with other contributions due to geometrical effects and straggling. From eq. (16) one deduces that equal effects from incident beam width and detector aperture are obtained at the surface for:

$$s \sin\alpha = d \sin\beta. \quad (18)$$

It is interesting to notice that the decrease of resolution due to straggling is compensated by the angular effects, and that for a good choice of parameters, the resolution does not depend very much on the depth over approximately 1 μm, which is another advantage in depth profiling when compared to RBS measurements. However, the previous calculation supposes a perfectly plane surface. It has been shown in RBS that surface roughness modifies the apparent surface resolution [16,17,18] and this effect is enhanced in ERD because of large incident and exit angles [19].

Fig. 2 shows the variation of the resolution $r(x)$ as a function of depth. It is shown that the geometry is predominant near the surface, whereas straggling and multiple scattering are more important for depths greater than 0.5 μm in the target that we have analysed.

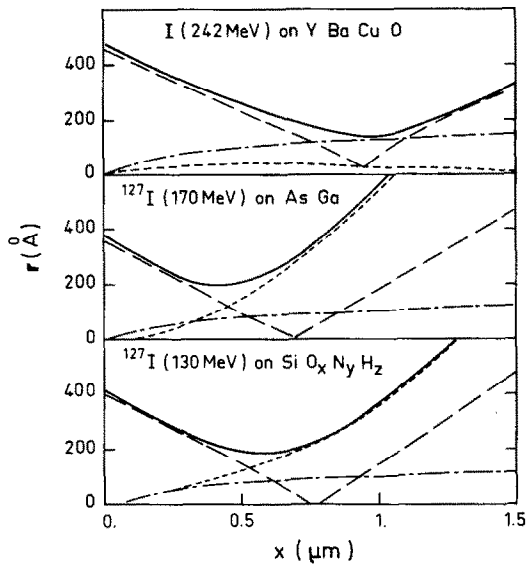

Fig. 2. Total calculated depth resolution (full line) for ^{127}I incident on SiONH ($\alpha = 5°$, $\beta = 35°$) and recoiling Si, on AsGa ($\alpha = 5°$, $\beta = 35°$) and recoiling As or Ga, on YBaCuO ($\alpha = \beta = 20°$) and recoiling Y. These calculations correspond to $d = 2$ mm, $s = 10$ mm and $D = 300$ mm used in the measurements (figs 4 to 7 and figs 11 to 14). Contributions from geometrical effects (long dashed line), multiple scattering (dashed-dotted line) and Bohr straggling (short dashed line) are represented for each case.

The resolution discussed above concerns one given element when it is well identified. We have also to consider the Z-resolution of the telescope. Figs. 3 and 4 illustrate the possibilities of our equipment: up to $A = 28$, the elements are separated over the analysed depth (1 μm). For heavier elements we see for example that for As ($A = 75$) and Ga ($A = 71$) the separation is

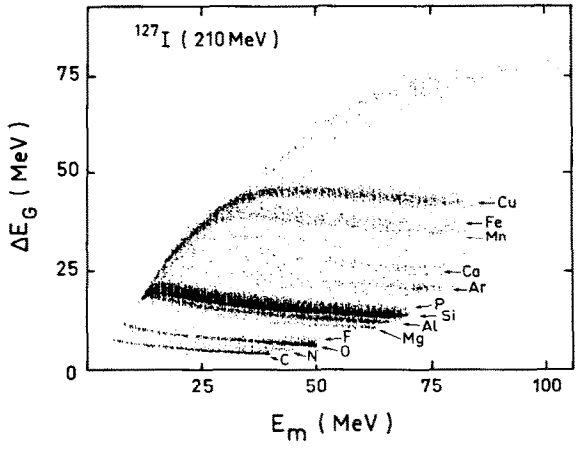

Fig. 3. Bi-parametric (E_m, ΔE_G) spectrum showing the Z discrimination for a large number of light and medium elements.

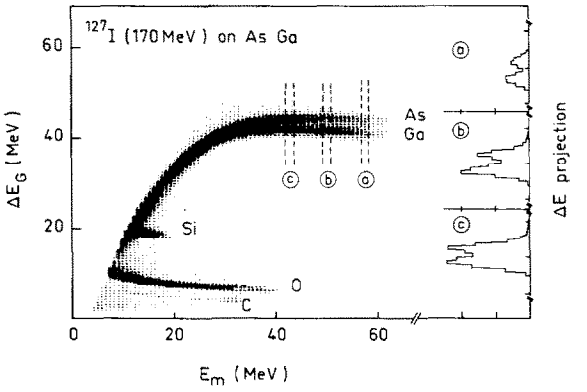

Fig. 4. Bi-parametric (E_m, ΔE_G) spectrum for a thin GaAs layer containing C traces, deposited on SiO_2. (a), (b) and (c) represent projections on the ΔE_G axis corresponding to depths 0, 2000 and 4000 Å.

achieved near the surface, but due to energy straggling and multiple scattering, the separation becomes impossible beyond 4000 Å.

2.4. Sensitivity

As the incident energy is below the Coulomb barrier, the Rutherford cross sections are used. It has been shown [20] that screening of the electrostatic potential of the nucleus by its atomic electrons can produce deviations from the Rutherford formulae in RBS, and the same effect holds for ERD. However, by analogy with the RBS treatment, we estimate this correction to be inferior to 1%.

2.5. Standard conditions

Performances concerning analysed depth, sensitivity and resolution cannot directly be compared in different experimental conditions. To have some estimates, we define a "standard" set of parameters which are used in calculations for comparison with other experimental arrangements [21]:

Beam
Intensity $i = 15$ nA (electrical);
Irradiation time: 2 hours.
Geometry:
$\alpha = \beta = 15°$, $d = s = 2$ mm, $D = 177$ mm ($\Omega = 10^{-4}$ sr).

Surface resolution δx_0
Neglecting the straggling in the entrance foil of the telescope, the surface resolution is given by the geometry

$$\delta x_0 = \frac{2kE_0\delta\beta_0}{\{S\}}. \tag{19}$$

Analysed depth e

A rough approximation is

$$e = \frac{1}{2}\frac{kE_0}{\{S\}}. \tag{20}$$

Minimum detection limit

This limit is determined by assuming a statistical limit of 30% (11 counts in the integrated peak) and a cross section given by the Rutherford scattering law.

Comparisons for different incident ions and energies are given in table 1. It appears that the resolution, analysed depth and detection limit are of the same order of magnitude in the different cases. This shows the interest of heavy incident ions of high energy which allow us to analyse all elements whereas light incident ions ($A < 35$) limit the analysis to light elements ($A \leq 30$) when Z_2 discrimination is made with a telescope. It can also been noticed [eq. (19) and (20)] that the ratio of analysed depth to surface resolution is a constant, and

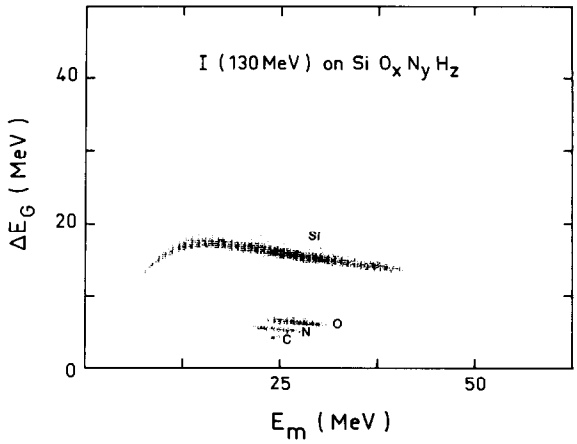

Fig. 5. Bi-parametric (E_m, ΔE_G) spectrum for a thin $SiO_xN_yH_z$ layer deposited on Si. Si, O, N, and C are completely resolved.

Table 1
Comparison of resolution, analysed depth and detection limit for various elements with different incident particles and energies. The calculations are made in the "standard" conditions (see text), neglecting the question of recoil discrimination.

Energy (MeV)	Incident particle	Target	Recoiling nucleus	Surface resolution (Å)	Analysed depth (μm)	Detection limit (10^{14} at./cm^2)
30	^{35}Cl	SiONH	Si	48	0.45	1.93
			O	64	0.60	2.93
			N	68	0.63	3.18
100	^{58}Ni	SiONH	Si	122	1.13	4.22
			O	151	1.40	5.69
			N	157	1.45	6.04
		AsGa	As, Ga	52	0.49	2.38
		YBaCuO	Ba	35	0.33	1.23
			Y	40	0.38	1.88
			Cu	45	0.41	2.54
			O	77	0.71	5.69
130	^{127}I	SiONH	Si	86	0.80	0.61
			O	98	0.91	0.72
			N	102	0.94	0.74
170		AsGa	As, Ga	66	0.61	0.82
242		YBaCuO	Ba	35	0.33	1.23
			Y	40	0.38	1.88
			Cu	45	0.41	2.54
			O	77	0.71	5.69
		BiSrCaCuO	Bi	58	0.54	0.72
			Sr	70	0.64	1.48
			Cu	78	0.72	1.69
			Ca	86	0.80	1.83
			O	113	1.04	2.50

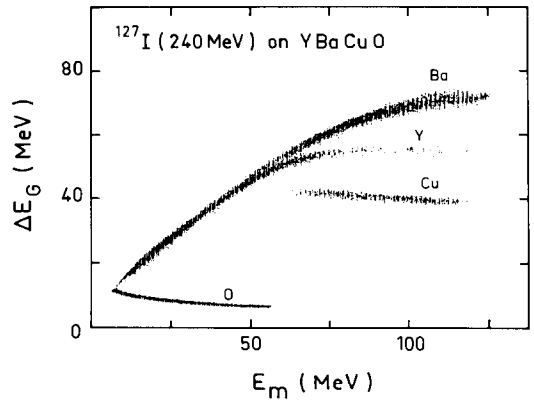

Fig. 6. Bi-parametric (E_m, ΔE_G) spectrum for a thin YBaCuO layer deposited on ZrO_2. Y and Ba are resolved for $E_m > 75$ MeV, corresponding to energies $E_0 > 135$ MeV.

can be considered, with the approximation used here, as independent of the type and of the energy of the incident particle.

2.6. Experimental conditions

The optimization of the incident energy and of the detection directions necessitates a compromise between several constants. The sensitivity is better for low incident energy, but the detecting system requires high energy for Z_2 separation as we can see in figs. 6 and 7. Detecting angles near 90° would give high sensitivity, but energy and resolution decrease for large angles. For $\alpha + \beta$ fixed, different relative values of α and β introduce other resolution and depth scales. Therefore, the optimal conditions cannot been deduced from a general discussion, but have to be defined in each case, depending on the thickness and composition of the target. We have profiled elements from carbon to bismuth with an incident beam of ^{127}I in the analysed layers of dielectric

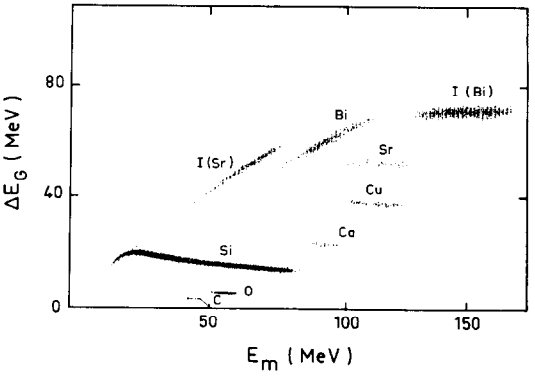

Fig. 7. Bi-parametric (E_m, ΔE_G) spectrum for a thin BiSrCaCuO layer deposited on Si. All recoiling atoms are resolved, and scattered I from Bi and Sr are also indicated.

$SiO_xN_yH_z$ (fig. 5) of hydrogenated amorphous semiconductor a-AsGa:H (fig. 4) and of superconductor films of YBaCuO (fig. 6) and BiSrCaCuO (fig. 7) in various experimental conditions (energy, geometry) which are indicated in table 2.

3. Experimental setup

3.1. Targets

Samples analysed by the ERD method have been provided by several groups which used different techniques of preparation. The $SiO_xN_yH_z$ targets were deposited on silicon substrates by PECVP (photon enhanced chemical vapor deposition) by the LEPES group (Laboratoire d'Etude des Propriétés Electronique des Solides, Grenoble). GaAs films were obtained by B. Despax (LGE-Toulouse) (Laboratoire de Génie Electrique) by Ga sputtering in a AsH_3 atmosphere. Superconductor thin films have been deposited in our laboratory by laser evaporation from bulk targets of YBaCuO and BiSrCaCuO, by using a pulsed excimer laser. Annealing at 850–900 °C has been performed in an oxygen atmosphere in order to obtain superconducting films.

3.2. Scattering chamber

Fig. 1 shows a schematic diagram of the detecting system and the geometry used in our measurements.

The 16 MV tandem accelerator of the CRN with a foil stripper delivers particles with an energy definition of 10^{-3}. The incident parallel beam is defined by circular collimators of 2 mm diameter. The target holder rotates on an axis perpendicular to the beam, and the detecting system can also rotate on this axis. The incident beam is measured in a Faraday cup behind the target. During the measurements, the beam stability is controlled on the current integrator, an absolute charge measurement being unnecessary for relative comparisons of elements in the same target.

The incidence and detecting angles can be changed from outside without modifying the vacuum conditions.

3.3. The ΔE(gas)–E(solid) telescope

The ΔE–E telescope represented on fig. 8 is similar to the one described by Barett [22]. The entrance foil is a 60 $\mu g/cm^2$ formvar foil and the bias voltages were +180 V for the anode and +70 V for the grid. The energy loss in formvar is shown on fig. 9 and can generally be considered to be negligible for all elements as compared to the total energy. The gas used is typically isobutane at a pressure of 30–50 Torr introduced in the ionization chamber through tubes at a constant flow with an external regulation which also insures

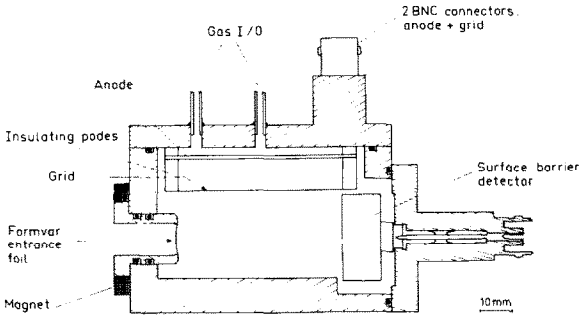

Fig. 8. Schematic representation of the E(solid)–ΔE(gas) telescope. The bias voltages used in the measurements were: anode: +180 V, grid +70 V.

constant pressure in the chambers. Energy losses in the gas are represented on fig. 10. The surface barrier detector which measures the residual energy has an active area of 100 mm^2 and a depletion depth of 300 μm.

3.4. Data acquisition and analysis

The data acquisition system on a HP1000 computer [23] is used to register all multiparametric events during the experiment. A two parameter (E_R, ΔE_G) spectrum is also displayed during the acquisition time in order to control and plot the data on line during operation. The complete data are registered in list mode on a magnetic tape for further detailed treatment.

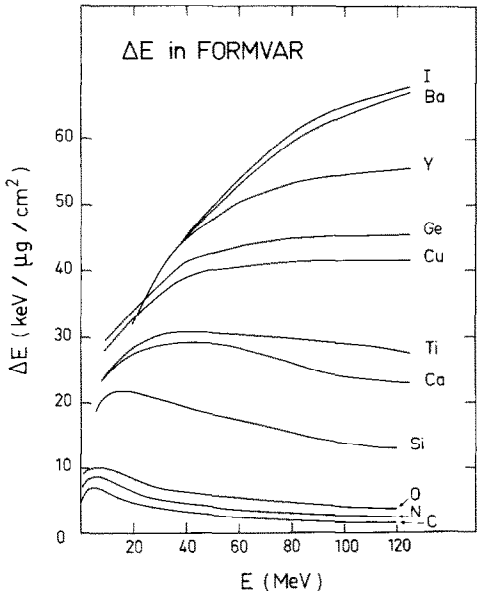

Fig. 9. Energy loss of different ions in formvar as a function of energy.

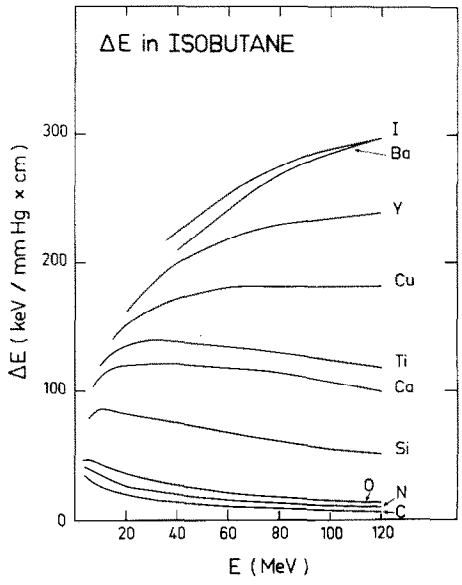

Fig. 10. Energy loss of different ions in the gas (isobutane) of the telescope as a function of energy.

The total two parameter spectra are reconstructed after the experiment. As E_R and ΔE_G are measured simultaneously, a more convenient representation is the biparametric ($E_m = E_R + \Delta E_G$, ΔE_G) spectrum that we have adopted. The gain of the E_R and ΔE_G amplifying chains being different, a matching factor f has to be determined to add the two terms. This can be done in two ways:

- the same target elements are measured with and without gas pressure in the ionization chamber. Comparison of the E_R and ΔE_G spectra gives the matching factor.
- E_R and ΔE_G can be calculated for given target elements at a known pressure. From the comparison with the measured values, one deduces the matching factor f.

In practice, the second method is more satisfying because we were confronted with problems with the linearity of the detectors as we will discuss later.

Examples of two parameter (E_m, ΔE_G) spectra are shown in figs. 3 to 7.

A monoparametric energy spectrum for each element is obtained by projection of the region delimited by a polygonal line corresponding to this element.

The last step in the treatment consists of the transformation of the energy spectrum $Y(E_m)$ into the profile. Assuming a given composition of the target, the energy loss per unit of length is calculated by using the tables of Ziegler [24] and Bragg's additivity rule. As the cross-sections depend also on the energy, and since the incident energy is below the Coulomb barrier, Rutherford cross-sections are used to renormalize the $N(x)$

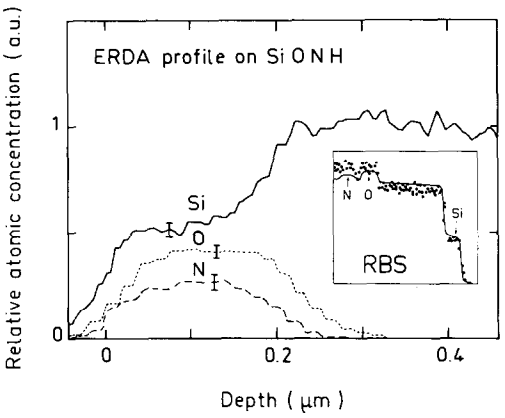

Fig. 11. Concentration profiles for the elements represented in fig. 5. The insert represents the RBS spectrum (points) measured with the same target, and a simulation (full line) calculated witl. the mean concentrations determined by ERD. Error bars indicate the uncertainties associated with counting errors.

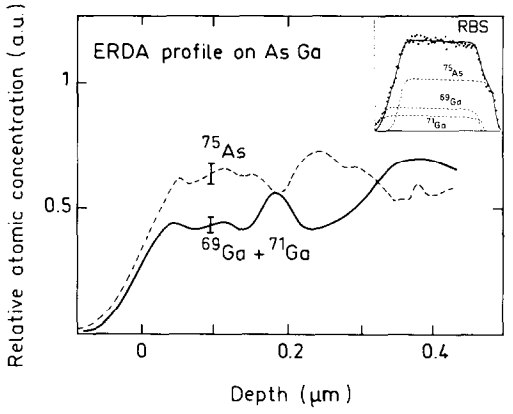

Fig. 12. Concentration profiles for As and Ga from fig. 4. The insert represents the RBS spectrum (points) measured with the same target, and a simulation (full line) calculated with the mean stoichiometries determined by ERD. The dashed lines of the RBS simulation show the mean contributions from each isotope. Error bars indicate the uncertainties associated with counting errors.

spectrum at each depth in order to deduce the profile $C(x)$.

Iterations on the stoichiometry can be performed if necessary. The principle is the same as the one used in RBS simulations as, for example RUMP [25] or similar programs [26,27,28] and consists in dividing the target in a succession of sublayers for the calculation. Fig. 11 shows the profiles deduced from the spectrum of fig. 5 for Si, O and N. Since the irradiation and geometrical conditions are the same for all the elements in the target, the relative concentrations are obtained directly as a function of depth by this method which is therefore very powerful for thin film analysis.

In fact, nuclear techniques are sensitivity to the areal mass ρt (where ρ is the density). Therefore, the density ρ has to be known to determine the depth scale in unit of length. For thin films, the density ρ is often assumed to be equal to that of bulk material, but on the other hand, if the film thickness is measured by another technique, for example ellipsometry, it is possible to deduce the effective density and absolute concentration for each element as a function of depth from ERD measurements.

4. Results and discussion

Figs. 11 to 14 show the profiles for three types of samples which have been analysed: $SiO_xN_yH_z$ for light elements, demonstrating the wide range of applicability of the ERD method with heavy ions. It is also shown that the Z_2 resolution decreases with increasing Z_2, all elements being resolved for $Z_2 \leq 15$.

It is seen in fig. 6 and 7 that there is a threshold for the discrimination of heavy ions with the telescope, situated approximately at 60 MeV for Cu and 75 MeV for Y and Ba. This corresponds to a minimum projectile energy of about 120–135 MeV for ^{127}I on Cu, Y or Ba. An even greater projectile energy is needed to separately depth profile the heavier elements.

Inserts in figs. 11 to 13 show the RBS spectra in each case, measured with a 3 MeV ^4He beam. As a test of consistency of our measurements, we made simulations of the RBS spectra with average concentrations obtained by ERD and the solid lines in the RBS inserts represent the curves calculated without any adjusted parameters.

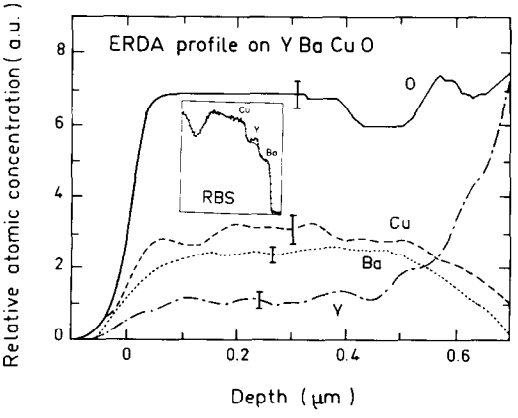

Fig. 13. Concentration profiles for YBaCuO (fig. 6). The insert represents the RBS spectrum (points) measured with the same target, and a simulation (full line) calculated with the mean stoichiometries determined by ERD. Error bars indicate the statistical uncertainty

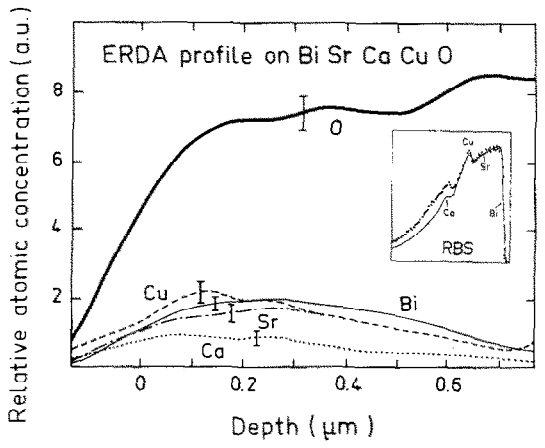

Fig. 14. Concentration profiles for BiSrCaCuO (fig. 7). The insert represents the RBS spectrum (points) measured with the same target, and a simulation (full line) calculated with the mean stoichiometries determined by ERD. Error bars indicate the statistical uncertainty.

The comparison of the ERD profiles with the RBS spectra clearly points out the advantages of the first method. In all the three cases studied, ERD allows peak separation in contrast to RBS where large overlapping regions appear, limiting RBS profiling to some heavy elements in the near surface region where surface contamination or oxydation could seriously alter the composition. However, in our experimental conditions, the RBS shows a better surface resolution than ERD. This is particularly apparent on fig. 13, where the RBS data indicates accumulation of *Y* on the surface, whereas the ERD *Y* spectrum does not exhibit such an enhancement, due to the decrease in resolution.

Table 2 shows the comparison between the ERD surface resolution as calculated with the theoretical expressions given in section 2, and the experimental values determined on the spectra of figs. 11 and 14. It should be noticed that, in order to improve the sensitivity, our experimental conditions do not correspond to the standard conditions used in section 2 for comparisons with other experimental arrangements (table 1). There is a satisfactory agreement for SiONH and GaAs targets but serious discrepancies appear for superconductors. This is attributed to the surface roughness and has been clearly seen, in particular by the scanning electron microscopy (SEM) of the BiSrCaCuO thin films heated above the melting point temperature (T_m = 865 °C) showing a surface morphology which is characteristic of melting–resolidification phenomena [29]. This is also confirmed by the RBS spectra. At normal incidence, surface irregularities appear on the low energy part of the spectrum corresponding to the interface, where they add to the normal straggling as thickness non-uniformities.

The hydrogen concentration profile in $SiO_xN_yH_z$ and a-AsGa : H are measured by conventional low energy ERD with a 3 MeV ^{4}He beam, after the determination of all other elements by high energy heavy ion ERD (or any other method). This procedure used for H measurements is justified because the H contribution to the stopping power, as compared to the other elements, can be considered as negligible in the calculations to a good approximation, thus avoiding time consuming iterations.

The thicknesses of the analysed samples are in the 2000–4000 Å range, and as a check were confirmed by other measurements (ellipsometry, RBS). However, due to the uncertainties on energy-loss data for heavy ions in solids, the precision on the thickness (and depth scale) suffers from an error which cannot be evaluate accurately; but it is almost greater than for RBS with α particles where an important effort has been made for stopping power determination, allowing the precision to reach a value generally estimated to be around 3%. In comparison, the film thickness obtained by ERD are in the 10% error limit, which could correspond to 10% precision in the stopping power tables for heavy ions.

Another possible source of error in the ERD technique with heavy ions concerns the energy calibration on which the depth scale depends. It is well known that Si surface barrier detectors exhibit a pulse height defect (PHD) when used with heavy ions [30]. The PHD is

Table 2
Comparison of experimental and calculated values of surface resolution for the samples represented in figs. 11 to 14. The detection geometry is defined by $s = 2$ mm, $d = 10$ mm, $D = 300$ mm. Differences between experiment and calculations a attributed to surface roughness.

Incident energy (MeV)	Target	Recoiling nucleus	Surface resolution (Å)	
			Experimental	Calculated
130	SiONH	Si	650	410
	$\alpha = 5°$	O	650	430
	$\beta = 35°$	N	650	430
170	AsGa	As	800	360
	$\alpha = 5°$	Ga	600	360
	$\beta = 35°$			
242	YBaCuO	Y	1200	450
	$\alpha = \beta = 20°$	Ba	900	400
		Cu	*700*	*520*
		O	700	800
242	BiSrCaCuO	Bi	2000	400
	$\alpha = \beta = 20°$	Sr	2000	500
		Ca	2000	650
		Cu	2000	550
		O	2000	900

defined as the difference between the true energy and that measured with the detector.

The PHD is the sum of three terms: the window defect Δ_w due to the energy loss in the entrance window, the nuclear stopping defect Δ_n due to non-ionizing nuclear collisions, and the residual defect Δ_r usually attributed to the recombination of electron–hole pairs in the plasma produced along the ionized track. Δ_w and Δ_n can be calculated easily, but the evaluation of the recombination is much more tedious. Semi-empirical formulae for PHD calculations have been established from systematic measurements [31], which depend on the mass, charge, energy and energy loss of the recoiling ion as well as on the resistivity and electric field strength characterizing the detector. One has therefore to choose detectors in which it is possible to establish large electric fields which are operate with the highest possible bias voltage in order to minimize the PHD. The effects are then negligible for light ions like C and O, and a calibration curve can be determined from which the PHD is deduced by extrapolation for heavier ions.

Using the calibration curve and comparing with the semi-empirical formula, one can deduce the behaviour of the PHD for the different ions at various energies, and evaluate the correction in each case and its influence on the depth scale. We found that a satisfying and convenient procedure consits in defining a linear calibration curve of the form

$$E_{m,i} = Ac + E_{0,i},$$

where c is the channel and A the energy dispersion (keV/channel) is the same for all recoiling atoms, whereas $E_{0,i}$ is adjusted for each ion to take into account the mean PHD for this ion over the energy range corresponding to the analysed depth and reproducing correctly the energy of recoils from the target surface.

Possible deterioration of the analysed films during irradiation could also introduce errors in the measurements due to sputtering at the surface or damage produced in the bulk. In the data reported here, beam intensities lower than 0.5 nA (particle) were used during short measuring times (< 15 min). Repeated profiling on the same sample gave no evidence for radiation-induced effects under these conditions, whereas damage in the thin films have been observed at higher intensities (> 10 nA particle). It has been shown in polymers [11] that under heavy ion irradiation the sensitivity to low concentrations of certain light elements is limited, and stripped off layers corresponding to sputtering rates of 1 Å/s have been seen with ^{127}I at 90 MeV [32]. But it is also known that the sensitivity to beam damage for polymers is several orders of magnitude higher than for other material, and we therefore expect that no dramatic change in the stoichiometry of the analysed thin films has been introduced by the incident beam.

5. Summary

We have presented results of depth profiling by the ERD method using high energy (up to 240 MeV) heavy ions (^{127}I) and a compact ΔE(gas)–E(solid) telescope detector to discriminate between different ions recoiling from the irradiated sample.

Depth resolution and detection limit dramatically depend on the geometry of the detection. We have shown that in the same geometrical conditions (called standard conditions in the text), the use of heavy ions (^{127}I) combined with a telescope extends the field of application of the ERD method to profiling of heavy elements, with approximatively constant characteristics for all elements: surface resolution ≈ 100 Å, analysed depth ≈ 1 μm and detection limit $\approx 10^{14}$ at/cm^2, comparable to the values obtained with ^{35}Cl (30 MeV) for light elements.

We have discussed this method in different experimental conditions to determine concentration profiles of dielectrics (SiONH) amorphous semiconductors (GaAs:H) and superconductors (YBaCuO, BiSrCaCuO) and demonstrated the improvements as compared to RBS. In practice, geometries different from the standard conditions were used to improve the counting rates, and surface resolution of ≈ 650 Å were measured on samples which are perfectly smooth. Furthermore, the method is very sensitive to surface roughness, and an important degradation of the resolution was measured on targets showing surface irregularities observed by electron microscopy.

References

[1] J. L'Ecuyer, C. Brassard, C. Cardinal, J. Chabbal, L. Deschênes, J.P. Labrie, B. Terreault, J.G. Martel and R. St. Jacques, J. Appl. Phys. 47 (1976) 381.
[2] B.L. Cohen, C.L. Fink and J.H. Degnan, J. Appl. Phys. 43 (1972) 19.
[3] S.S. Klein, Nucl. Instr. and Meth. B15 (1986) 464.
[4] B.L. Doyle and P.S. Peercy, Appl. Phys. Lett. 34 (1979) 11.
[5] R. Groleau, S.C. Gujrathi and J.P. Martin, Nucl. Instr. and Meth. 218 (1983) 11.
[6] M. Petrascu, I. Berceanu, I. Brancus, A. Buta, M. Duma, C. Grama, I. Lazar, I. Mihai, M. Petrovici, V. Simon, M. Mihaila and I. Ghita, Nucl. Instr. and Meth. B4 (1984) 396.
[7] B.L. Doyle, P.S. Peercy, Tom J. Gray, C.L. Cocke and E. Justiniano, IEEE Trans. Nucl. Sci. NS-30 (1983) 1252.
[8] C.R. Gosset, Nucl. Instr. and Meth. B15 (1986) 481.
[9] H.J. Whitlow, G. Possnert and S. Petersson, Nucl. Instr. and Meth. B27 (1987) 448.
[10] H. Nagai, S. Hayashi, M. Aratani, T. Nozaki, M. Yanokura, I. Kohno, O. Kuboi, and Y. Yatsurugi, Nucl. Instr. and Meth. B28 (1987) 59.

[11] A.M. Behrooz, R.L. Headrick, L.E. Seiberling and R.W. Zurmuhle, Nucl. Instr. and Meth. B28 (1987) 108.
[12] T.W. Conlon, Nucl. Instr. and Meth. B9 (1985) 311.
[13] G. Ross and B. Terreault, J. Appl. Phys. 51 (1980) 1259.
[14] P. Sigmund and K.B. Winterbon, Nucl Instr. and Meth. 119 (1974) 541.
[15] A.D. Marwick and P. Sigmund, Nucl. Instr. and Meth. 126 (1975) 317.
[16] K. Schmid and H. Ryssel, Nucl. Instr. and Meth. 119 (1974) 287.
[17] A.R. Knudson, Nucl. Instr. and Meth. 168 (1980) 287.
[18] K.D. Edge and U. Bill, Nucl. Instr. and Meth. 168 (1980) 157.
[19] B.L. Doyle and D.K. Brice, Nucl. Instr. and Meth. B35 (1988) 301.
[20] J. L'Ecuyer, J.A. Davies and N. Matsunami, Nucl. Instr. and Meth. 160 (1979) 337.
[21] S.C. Gujrathi, P. Aubry, L. Lemay and J.P. Martin, Can. J. Phys. 65 (1987) 975.
[22] J. Barett, Nucl. Instr. and Meth. 126 (1975) 181.
[23] G. Zehnacker, Synus - Système Nucléaire de Strasbourg-Internal Publication (1986).
[24] J.F. Ziegler, Handbook of Stopping Cross-Section for Energetic Ions in all Elements, Vol. 5 (Pergamon, 1980).
[25] L.R. Doolittle, Nucl. Instr. and Meth. B9 (1985) 344, Nucl. Instr. and Meth. B15 (1986) 227.
[26] W.Z. Li and Z. Al-Tamimi, Nucl. Instr. and Meth. B15 (1986) 241.
[27] J.W. Butler, Nucl. Instr. and Meth. B15 (1981) 232.
[28] Y. Kido and Y. Oso, Nucl. Instr. and Meth. B9 (1985) 291.
[29] E. Fogarassy, C. Fuchs, P. Siffert, J. Perrière, X.Z. Wang and F. Rochet, Sol. State Commun. V. 67(10) (1988) 975.
[30] J.J. Grob, Thèse, Strasbourg (1979).
[31] M. Oghihara, Y. Nagashima, W. Galtser and T. Mikumo, Nucl. Instr. and Meth. A251 (1986) 313.
[32] B. Sundqvist, private communication.